ELSEVIER

Applied Catalysis A: General 230 (2002) 233–243

APPLIED CATALYSIS A: GENERAL

www.elsevier.com/locate/apcata

Liquid phase benzoylation of arenes over iron promoted sulphated zirconia

H. Suja, C.S. Deepa, K. Sreeja Rani, S. Sugunan*

Department of Applied Chemistry, Cochin University of Science and Technology, Kochi-22, Kerala, India

Received 10 September 2001; received in revised form 12 December 2001; accepted 12 December 2001

Abstract

The present work undertakes the preparation and physico-chemical characterisation of iron promoted sulphated zirconia (SZ) with different amounts of iron loading and their application to Friedel–Crafts benzoylation of benzene, toluene and xylene under different experimental conditions. XRD and laser Raman techniques reveal the stabilisation of the tetragonal phase of zirconia and the existence of iron in highly dispersed form as Fe_2O_3 on the catalyst surface. The surface acidic properties were determined by ammonia temperature programmed desorption (TPD) and perylene adsorption. The results were supported by the TGA studies after adsorption of pyridine and 2,6-dimethylpyridine (2,6-DMP). Strong Lewis acid sites on the surface, which are evident from TPD and perylene adsorption studies, explain the high catalytic activity of the systems towards benzoylation. The experimental results provide evidence for the truly heterogeneous nature of the reaction. The studies also establish the resistance to deactivation in the metal incorporated sulphated systems.

Keywords: Iron promoted sulphated zirconia; Perylene adsorption studies; Friedel–Crafts benzoylation

1. Introduction

Friedel–Crafts acylation constitutes the most important method for the preparation of aryl ketones. A wide range of homogeneous catalysts like $FeCl_3$, $AlCl_3$, BF_3 and protonic acids like HF and H_2SO_4 have been found to be well suited for the reaction [1,2]. These catalysts, however, suffer from the inherent drawback of extreme corrosivity, high susceptibility to water and difficulty in catalyst recovery. The stoichiometric amounts of the catalyst with respect to the benzoylating agent required for the reaction makes the work-up procedure tedious. The high Lewis acidity of these homogeneous catalysts also results in several undesirable side reactions leading to multiple acylated products. The rampant use of acid catalysts in chemical and refinery industries has resulted in extensive environmental pollution during the past few decades. Growing ecological concern demands the replacement of highly corrosive, hazardous and polluting liquid acids by eco-friendly solid acids. A wide range of solid acids from zeolites [3,4] and clays [5] to Nafion-H [6] has been scanned for their applicability towards this reaction.

Recently, much attention has been centered on the sulphate doped metal oxide catalysts, the superacidity of which has been a subject of debate. These systems have been reported to be active for the benzoylation of toluene with benzoyl chloride and benzoic anhydride at temperatures below the reflux temperature of the mixture [7,8]. However, sulphur leaching during the reaction, coke deposition at high temperatures, changes in sulphur oxidation state and phase

* Corresponding author. Fax: +91-484-532495.
E-mail address: ssg@cusat.ac.in (S. Sugunan).

0926-860X/02/$ – see front matter
PII: S0926-860X(02)00004-2

changes from tetragonal to monoclinic limit the industrial use of this catalyst. Constant efforts are on the way to improve the stability and reusability of the systems. Incorporation of transition metal oxides has been reported to enhance the thermal stability and the stability of the surface sulphate species [9]. Reports of iron promoted sulphated zirconia (SZ) are available [10,12]. We attempted an exhaustive investigation of the physico-chemical characterisation of iron promoted SZ with different metal loadings, giving special emphasis on the acidity evaluation, a concept overlooked in most of the earlier works. We also report the acylation of benzene, toluene and xylene over these catalytic systems. The applicability of iron-incorporated SZ systems for acylation has not been explored so far. The influence of reaction temperature and substrate-to-acylating agent molar ratio on the activity and selectivity has also been investigated in detail. The interest in our catalyst systems stems from its environmentally friendly nature and its ease of handling. The thermal and chemical stability of the system, along with its high Lewis acidity, reusability and resistance to deactivation, renders it a promising catalyst for Friedel–Crafts acylation of aromatics.

2. Experimental

2.1. Catalyst preparation

Hydrous zirconium oxide was prepared by the hydrolysis of zirconyl nitrate (CDH) using aqueous ammonia under vigourous stirring at 80 °C and at pH 10. The precipitate was filtered, washed and dried overnight at 120 °C. Iron promoted SZ were prepared from the hydroxide by a single step impregnation using 1 N H_2SO_4 solution (10 ml/g of hydrous zirconium oxide) and ferric nitrate solution. The metal loading was varied from 2 to 10%, as indicated in the parentheses in sample notation. The samples, after overnight drying at 120 °C, were calcined at 700 °C for 3 h.

2.2. Physico-chemical characterisation

Surface area and pore volume of the catalysts were measured using BET method in a micromeritics Gemini surface area analyser by low temperature nitrogen adsorption. The crystallinity was determined by the powder XRD method in a Rigaku D-max C X-ray diffractometer using Ni filtered Cu Kα radiation (λ = 1.5406 Å). The thermal stability of the systems was examined using a Shimadzu thermogravimetric analyser (TGA-50) in nitrogen atmosphere at a heating rate of 20 °C/min. The IR spectrum of the sample was recorded on a Shimadzu spectrophotometer (DR 8001). The surface scan was carried out by laser Raman spectroscopic analysis (Dilor–Jobin spectrophotometer). The sulphate content was obtained by EDX analysis (Stereoscan 440).

The evaluation of surface acidity was carried out by temperature programmed desorption (TPD) of ammonia and electron acceptor studies using perylene. TPD of ammonia enabled the determination of the acid strength distribution. For TPD studies, pelletised catalyst was activated at 700 °C inside the reactor under a nitrogen flow for 0.5 h. After cooling to room temperature, ammonia was injected in the absence of the carrier gas flow and the system was allowed to attain equilibrium. The excess and physisorbed ammonia was flushed out by a current of nitrogen. The temperature was then raised in a step-wise manner at a linear heating rate of about 20 °C/min. The ammonia desorbed from 100 to 600 °C at intervals of 100 °C was trapped in dilute sulphuric acid solution and estimated volumetrically by back titration with NaOH.

Electron acceptor studies were carried out by stirring a weighed amount of the catalyst with different concentrations of perylene in benzene solvent. The amount of perylene adsorbed was determined by measuring the absorbance of the solution in a UV–VIS spectrophotometer (Shimadzu UV-160 A) before and after adsorption. The limiting amount of perylene adsorbed was obtained from Langmuir plots.

The acidity determination was supported by the TGA studies using pyridine and 2,6-dimethylpyridine (DMP) as probe molecules. The activated samples were kept in a dessicator containing pyridine/2,6-DMP under vacuum for 48 h to allow equilibrium adsorption and then subjected to thermal analysis in N_2 atmosphere at a heating rate of 20 °C/min.

2.3. Catalytic activity

The liquid phase benzoylation of benzene, toluene and xylene using benzoyl chloride was carried out in a 50 ml double-necked flask fitted with a spiral

condensor. The temperature was maintained using an oil bath. In a typical run, the aromatic substrate (benzene, toluene or xylene as the case may be) and benzoyl chloride in the specific molar ratio was added to 0.1 g of the catalyst in the round bottom flask and the reaction mixture was magnetically stirred. The product analysis was done using a Chemito 8610 gas chromatograph equipped with a flame ionisation detector and an SE-30 column. The aromatic substrate being taken in excess, the yields were calculated based on the amount of acylating agent. The selectivity for a product is expressed as the amount of the particular product divided by the total amount of products and multiplied by 100.

The influence of the reaction temperature on the reactivity and selectivity were also subjected to investigation. The catalyst activity was also screened for different molar ratios of toluene and benzoyl chloride. The present work also attempts a closer look into the metal leaching and deactivation of the systems under the reaction conditions to obtain a better understanding of the nature and course of the reaction.

3. Results and discussion

3.1. Catalyst characterisation

The surface area values for pure and SZ samples are presented in Table 1. The enhancement in the surface area of the sulphated samples can be explained on the basis of the higher resistance to sintering acquired via sulphation [13]. The dispersion of Fe_2O_3 particles causes a further rise in the surface area value. An increase in iron loading did not have a remarkable influence on the surface area. A slight lowering observed in the surface area values may be a result of the agglomeration of the iron particles at high metal loadings.

Consistent with the earlier reports [13], XRD data supports the stabilisation of the catalytically active tetragonal phase and retardation of crystallisation after incorporation of sulphate and iron species. In comparison with pure ZrO_2, the XRD patterns of sulphated and iron-incorporated zirconia samples showed an enrichment of the tetragonal phase (Fig. 1). The bulk structure of SZ remains virtually unchanged by the incorporation of promoters except for a lowering in crystallinity. The lowering of crystallinity becomes prominent with increased iron loading. The absence of the characteristic peaks of Fe_2O_3, implies the high dispersion of the iron particles on the zirconia surface. Traces of monoclinic phase detected along with a predominant tetragonal phase in SZ and low loaded FeSZ samples may be attributed to the high sulphate loadings in these systems. The special stability of the tetragonal phase diminishes at high sulphate loadings [14]. At high iron loadings, the monoclinic phase disappears completely, indicating the stabilisation of the tetragonal phase aided by the dispersion of Fe_2O_3 particles and the reduction of sulphate content, as shown by EDX analysis.

The sulphate content as obtained by EDX analysis is presented in Table 1. Incorporation of iron significantly improves the sulphate retaining ability. The sulphate content higher than that required for monolayer coverage implies the migration of the sulphate moieties into the bulk [14]. The bulk sulphate species may be retained to a greater extent when compared to the surface species during high temperature calcination. A slight lowering of the sulphate content was observed at high iron loadings. It may be assumed that the dispersion of iron particles restricts the sulphate species

Table 1
Physico-chemical properties—a comparative evaluation

Catalyst systems	Surface area (m^2/g)	Pore volume (cm^3/g)	Sulphate content (wt.%)	Sulphate retained (%)	Total acidity (amount of NH_3 desorbed, mmol/g)	Perylene adsorbed (10^{-6} mol/g)
ZrO_2	32.68	0.0654	–	–	0.307	0.085
SZ	44.81	0.0786	18.54	47.6	1.045	2.753
Fe(2)SZ	61.09	0.0821	30.10	84.70	1.2349	3.673
Fe(4)SZ	60.43	0.0830	28.86	81.29	1.2361	4.183
Fe(6)SZ	59.58	0.0846	27.13	76.42	1.2555	7.373
Fe(8)SZ	57.29	0.0745	24.65	69.44	1.2635	8.845
Fe(10)SZ	55.65	0.0882	23.05	64.93	1.3013	10.688

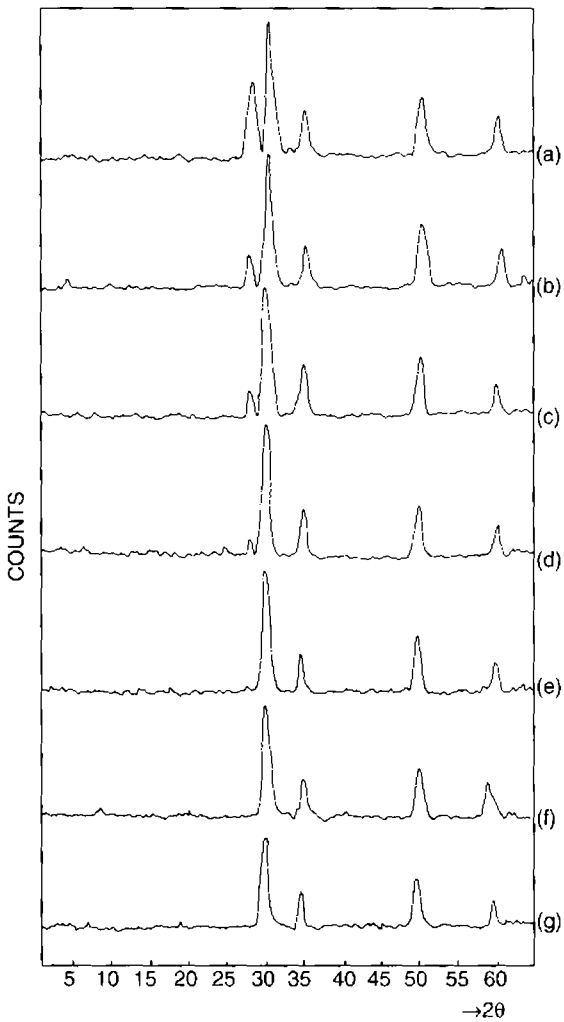

Fig. 1. XRD patterns of pure and modified zirconia samples: (a) ZrO_2; (b) SZ; (c) Fe(2)SZ; (d) Fe(4)SZ; (e) Fe(6)SZ; (f) Fe(8)SZ; (g) Fe(10)SZ.

more or less to the surface, minimising their migration into the bulk, which facilitates their easy removal during high temperature calcination.

The IR analysis of the sample reveals a broad peak with shoulders at around 1200 cm^{-1}, corresponding to the S–O mode of vibration. The peaks at 1029, 1076 and 1222 cm^{-1} are typical of a chelating bidentate sulphate species co-ordinated to a metal cation [15] (Fig. 2). The peak at 1380 cm^{-1} arises from the covalent character of S=O on a highly dehydrated oxide surface. The absence of any peak around 1400 cm^{-1} suggests the absence of polynuclear sulphate species [16] in spite of the high sulphate loading. A broad band due to the –OH species appears around 3479 cm^{-1} for pure zirconia, whereas for sulphated and iron promoted samples, the peak maxima was shifted to 3429 cm^{-1}. This shift in the –OH peak to a lower stretching frequency suggests the enhancement in acid strength for the sulphated samples. The increase in Bronsted acidity during sulphation may be ascribed to the generation of S–OH groups [17] or to the acidity enhancement of the surface –OH groups [18]. However, specific IR bands characteristic of bisulphate OH are difficult to detect due to their hydrogen bonding to the surface. So the specific categorisation of the –OH band as bisulphate group or as surface –OH becomes difficult.

Laser Raman spectroscopic results (Fig. 3) of the representative samples recorded complements the XRD and IR results. The peaks at 336, 370 and 472 cm^{-1} clearly indicates the predominance of monoclinic phase of ZrO_2 in pure sample. This, however, contradicts the XRD results, according to which tetragonal phase dominates. This can be rationalised if one bears in mind the fact that laser Raman spectroscopy is a surface characterisation technique while XRD remains a tool for the bulk analysis. The surface seems to be predominated by the monoclinic phase while the bulk remains as tetragonal. In the case of modified zirconia samples, a broadening of peaks was observed indicative of low crystallinity. The broadening of peaks also creates some uncertainty regarding the correct assignment of the peak positions to the respective crystalline phases. In sulphated and iron-incorporated samples with low metal loading (Fe(2)SZ), along with low intensity monoclinic bands, additional peaks appeared at 148, 270, 466, 624 cm^{-1} representing the tetragonal phase of zirconia [10,11,19]. This lends support to the reported stabilisation of the tetragonal phase [13] by sulphate modification. In samples with higher iron content, the monoclinic phase was completely absent. Peaks due to S–O and S=O stretching modes of surface sulphate species show up near 1059 and 1319 cm^{-1}, respectively [10]. The high intensity of the S–O band points to the high sulphate content in the samples. The poor resolution of the peak at 1319 cm^{-1}, makes the complete characterisation of sulphate co-ordination impossible. The lack of a significant change in the peak position after metal incorporation indicates that

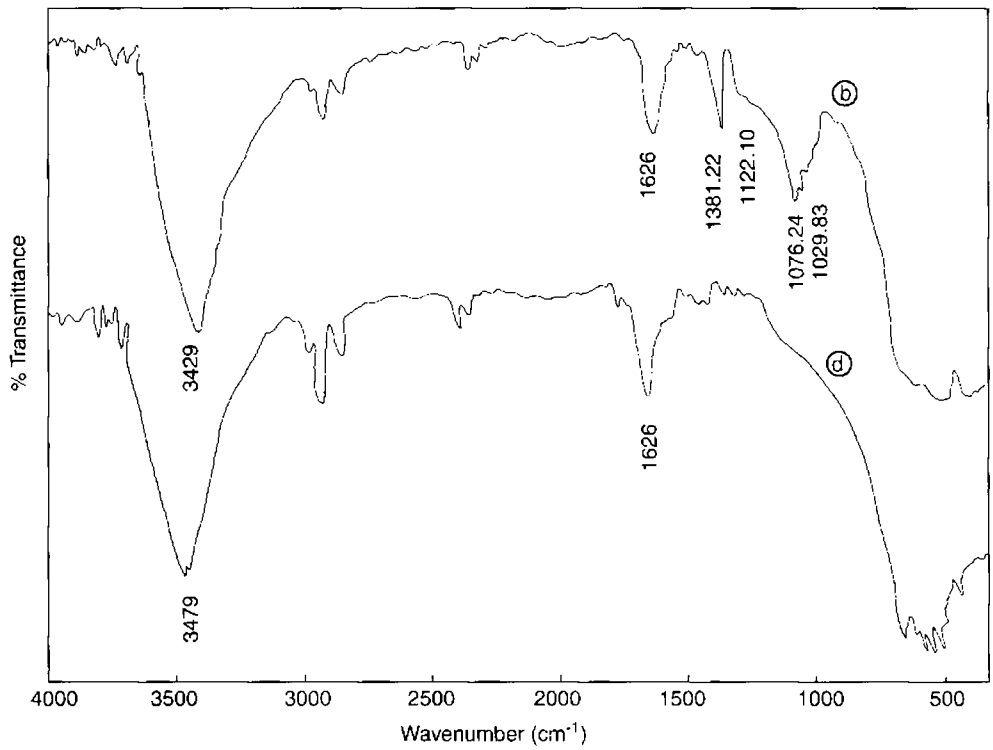

Fig. 2. IR spectra of pure and modified zirconia samples: (a) ZrO_2; (b) Fe(2)SZ.

the sulphate structure remains unaltered by addition of promoters. The Raman spectra also reveal the presence of iron dispersed as Fe_2O_3. The peaks at 300, 224 and 409 cm^{-1} correspond to the literature data for Fe_2O_3 [10]. In comparison with the spectrum of Fe(2)SZ, the peaks at 300, 224 and 409 cm^{-1} were more prominent for Fe(10)SZ, signifying the higher iron content.

The TGA confirms the thermal stability of the systems. Sulphate decomposition in simple SZ was observed at around 650 °C, whereas for iron-incorporated systems, the decomposition peak was shifted to around 750 °C. The higher thermal stability of the iron-incorporated systems also explains their high sulphate content. An increase in the iron loading did not have any significant effect on the sulphate decomposition temperature.

3.2. Acidic properties

The TPD of ammonia [20] was used to characterise the acid site distribution and furthermore to obtain the quantitative amounts of acid sites in the specified temperature range. The distribution pattern can be classified into weak (desorption at 100–200 °C), medium (200–400 °C) and strong (400–600 °C) acid sites. A broadening of the distribution curve was observed for pure ZrO_2 asymmetric on the high temperature side with a maximum at around 500 °C. The acid site distribution profiles for the modified zirconia samples exhibits two distinct maxima at around 300 and 500 °C, respectively (Fig. 4). Considerable enhancement of both strong and weak acid sites was observed after incorporation of sulphate and iron moieties. Only a slight enhancement was observed in the total acidity values of SZ and FeSZ systems in spite of the fact that the iron-incorporated samples had almost double the sulphate content when compared to simple sulphated system (Table 1). This clearly indicates that the sulphate content alone is not the deciding factor for the acidity and catalytic activity of the samples. The incorporation of promoters results in a rearrangement in the acid strength distribution in a direction

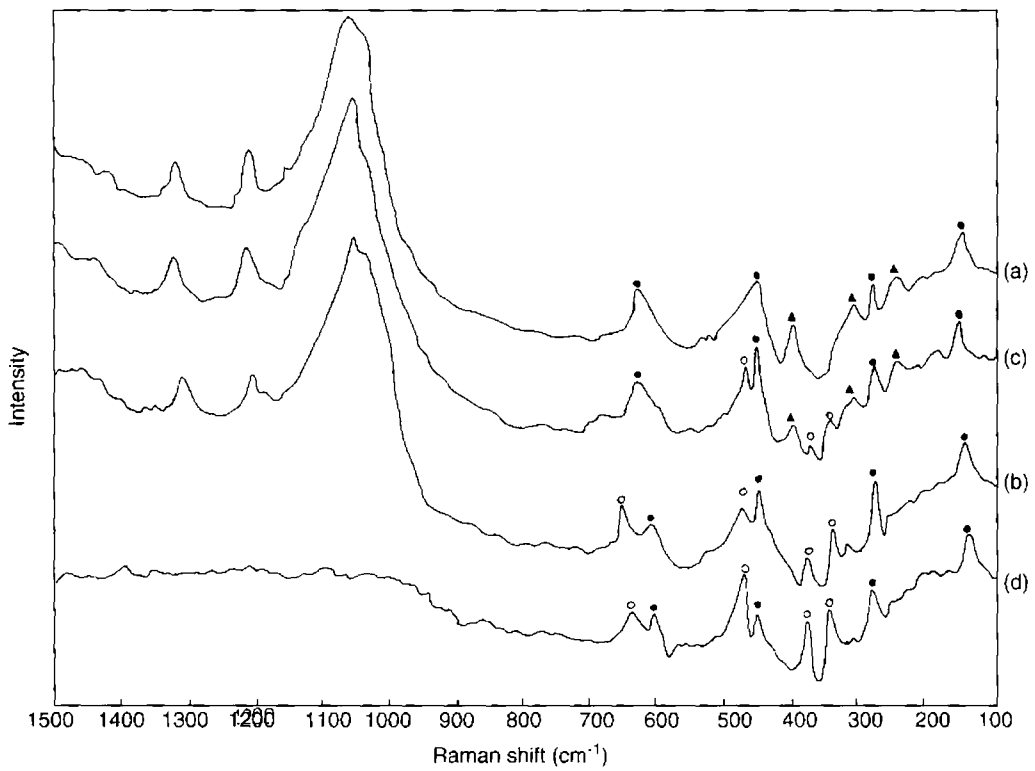

Fig. 3. Laser Raman spectra of representative samples: (a) ZrO_2; (b) SZ; (c)Fe(2)SZ; (d)Fe(10)SZ, (○): monoclinic; (●): tetragonal; (▲): Fe_2O_3.

favouring the formation of strong acid sites. The distribution change may be a coupled effect of the crystalline and structural changes. The amount of ammonia desorbed and hence the total acidities for the different iron promoted samples were also comparable. However, a significant difference was observed in the distribution pattern. A well-defined enhancement of the strong acid sites at the expense of weak ones with an increase in the iron loading is quite evident from the TPD profiles.

Adsorption studies using perylene as electron donor gives information regarding the Lewis acidity in presence of Bronsted acidity [21,22]. The technique is based on the ability of the catalyst surface site to accept a single electron from an electron donor like perylene to form charge transfer complexes. The perylene adsorption was done at room temperature from a solution in benzene. Perylene after electron donation gets adsorbed on the catalyst surface as radical cation. The limiting amount of perylene adsorbed, which gives a measure of the Lewis acidity or the electron-accepting capacity, was obtained from the Langmuir plot. The Lewis acidity enhancement can be ascribed to the increase in the electron acceptor properties of the three co-ordinate zirconium cations via the inductive effect of the sulphate anions, which withdraw electron density from the zirconium cations through the bridging oxygen atom. Incorporation of iron enhances the acid strength via electronic interactions. Introduction of the metal cation into the crystal lattice may result in the formation of some complex structures (Scheme 1) in some local areas on the surface.

According to the principle of electronegativity equalisation proposed by Sanderson [23], the electronegativity S_{int} of the complex structure and the partial charge δ_{Zr} on Zr^{4+} can be written as

$$S_{int} = [S_M^X S_{Zr} S_S S_O^Z]^{1/2+X+Z}$$

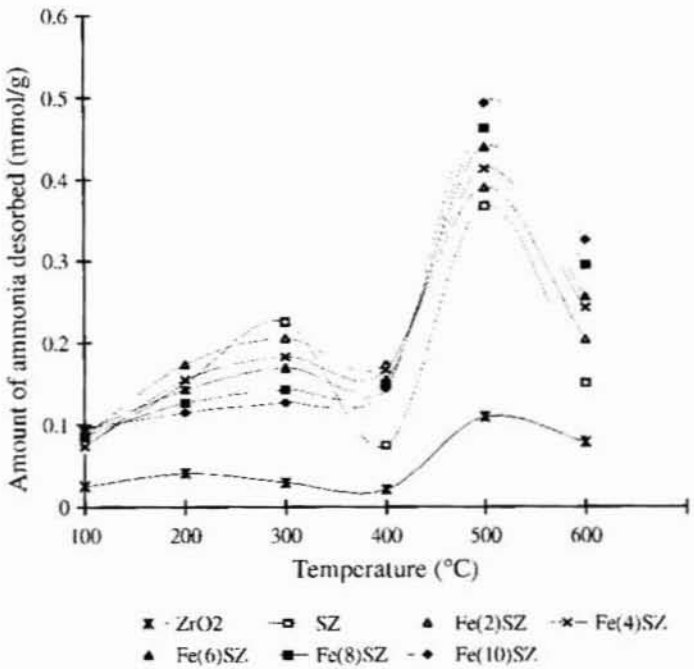

Fig. 4. Acid site distribution profiles from ammonia TPD.

$$\delta_{Zr} = \frac{S_{int} - S_{Zr}}{2.08\, S_{Zr}^{1/2}}$$

where S_M, S_{Zr}, S_S and S_O are the electronegativities of M, Zr, S and O while X and Z represent the numbers of M and O in the neighbourhood of Zr^{4+}. The electronegativity of Fe^{3+} being larger than that of Zr^{4+}, the electronegativity of the surface complex, S_{int} is increased and δ_{Zr} becomes more positive when Fe is introduced, thereby resulting in enhanced Lewis acidity. This also explains the increase in Lewis acidity at higher iron loadings (Table 1). Incorporation of iron in higher concentrations leads to the development of more and more localised complex structures, thereby contributing to an overall increase in the Lewis acidity.

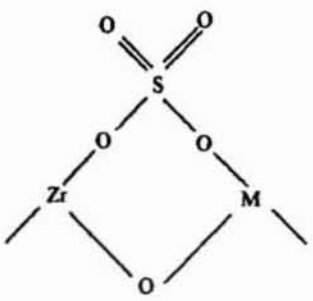

Scheme 1.

The TG pattern of the samples was recorded after adsorption of pyridine and 2,6-DMP to have a better understanding of the nature of surface acidity. Desorption was noted till the calcination temperature of 700 °C, since the distinct assignment of the weight decrease to pyridine/DMP desorption or sulphate decomposition or even dehydroxylation becomes impossible above the calcination temperature. The results are presented as percentage of pyridine/DMP desorbed in the specific temperature range (Fig. 5).

Pyridine (Py) adsorption was carried out to support the TPD data. The applicability of pyridine as probe to superacids and binary oxide catalysts has been demonstrated [24]. Since pyridine is adsorbed at the Lewis and the Bronsted sites, such an adsorption does not allow the differentiation between the two, but it provides a rough estimate of the total acidity. The TG curves after pyridine adsorption showed a continuous weight loss in the region from ambient to 700 °C. The

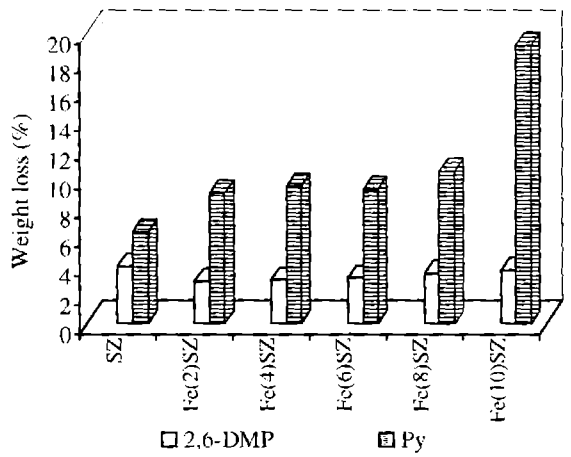

Fig. 5. Thermodesorption studies using pyridine and 2,6-DMP.

sharp weight loss observed in the high temperature region may be due to the oxidative decomposition of sulphate species by interaction with pyridine. The total percentage weight loss was almost constant for the iron-incorporated samples except for Fe(10)SZ, supporting the TPD results. The anomalous increase in the percentage weight loss observed for Fe(10)SZ may be a consequence of the lowering of the sulphate decomposition temperature at high iron loading. The interaction of sulphated iron oxide and pyridine has been reported earlier [25].

The thermodesorption study of 2,6-DMP was carried out with an intention of obtaining a comparative evaluation of the Bronsted acidity in the samples. The possibility of the chemisorption of sterically hindered dimethyl and *tert*-butyl pyridines as proton specific probes for the selective characterisation of the Bronsted acid sites has been suggested [26,27]. The formation of weak bonds between 2,6-DMP and Lewis acid sites has been observed in alumina, boron phosphates and zeolites [26,28]. The IR bands corresponding to Lewis site-associated DMP disappeared with an increase in desorption temperature [26]. Dewing et al. [29] have also suggested the presence of "special" Lewis sites in γ-alumina for which sterically hindered pyridines do not show any hindrance. The importance of the purging temperature for selective adsorption of 2,6-DMP on Bronsted acid sites has been previously reported [30]. 2,6-DMP is believed to be held co-ordinatively on the Lewis acid sites at lower temperature due to the rather weak effect of the steric hindrance due to the methyl groups in the neighbourhood of the basic sites of pyridine. Satsuma et al. [30] also reported a complete elimination of the co-ordinatively adsorbed 2,6-DMP on Lewis acid sites after purging at an appropriate temperature (above 573 K). Thus, we presume the amount of 2,6-DMP desorbed at temperatures above 300 °C to be due to desorption from Bronsted acid sites. Taking a cumulative plot, the amount of 2,6-DMP desorbed showed a trivial increase with increase in the iron loading. This we take as an approximate measure of the Bronsted acidity. The low percentage values can be due to the trace amount of Bronsted acidity left after high temperature calcination or it may be a consequence of neglecting the desorption at lower temperatures.

3.3. Catalytic properties

Benzoylation of arenes proceeded very efficiently over iron promoted SZ systems. Pure ZrO_2 and SZ exhibited poor reactivity (around 3 and 34%, respectively) towards benzoylation of toluene at the refluxing temperature, which can be explained on the basis of their low acidity values. The higher activity of the iron promoted systems may be attributed to the redox properties of iron as well as its strong acidity, as evident from TPD studies. Thermodesorption of 2,6-DMP predicts a trivial enhancement in the Bronsted acidity with increasing iron content, whereas perylene adsorption studies provide clear evidence for a distinct enhancement of Lewis acidity upon increasing the iron loading. The marginal enhancement in Bronsted acidity value seems quite inadequate for explaining the increase in the catalytic activity. However, the Lewis acidity enhancement predicted by perylene adsorption studies parallels the steady increase in reactivity observed with the increase in the percentage iron composition (Table 2). This suggests a dominating role of the Lewis acid sites in deciding the catalytic activity of the various systems towards benzoylation.

The active participation of the Lewis acid sites in the benzoylation reaction is also supported by the catalytic activity studies at different calcination temperatures of the catalyst (Table 3). The increase in the catalytic activity observed with increasing calcination temperature parallels the enhancement of Lewis acidity of the samples obtained by perylene adsorption

Table 2
Benzoylation of toluene over pure and modified zirconia systems

System	Time (min)	Conversion (%)	Selectivity (%)	
			Ortho	*Para*
ZrO_2	60	3.45	–	100
SZ	60	34.35	16.12	83.88
Fe(2)SZ	60	79.61	15.16	84.84
Fe(4)SZ	60	88.56	15.85	84.15
Fe(6)SZ	60	96.49	15.38	84.62
Fe(8)SZ	45	100	14.95	85.05
Fe(10)SZ	30	100	14.43	85.57

Reaction temperature: 110 °C; 0.1 g catalyst; molar ratio (toluene:benzoyl chloride) 5:1.

results. IR studies on adsorbed pyridine by Morterra et al. [31] supports the gradual elimination of all but a small fraction of the Bronsted acid sites after high temperature calcination and the reversible transformation of Lewis to Bronsted acidity upon exposure of the sample to moisture. A considerable loss in activity observed when the catalyst was exposed to moisture lends support to the proposed involvement of the Lewis acid sites in catalysing the reaction.

Benzoylation of benzene, toluene and xylene was carried out at the corresponding refluxing temperatures for 1 h over Fe(2)SZ system. The reactivities were in the order: benzene (15.37%) < toluene (79.61%) < xylene (96.23%). This can be well explained on the basis of the *ortho–para* directing effect of the alkyl substituent on the aromatic ring. The electron-releasing nature of the alkyl groups favour the electrophilic substitution at the aromatic nucleus. The *para* substitution predominates due to the bulky nature of the acyl group. Only mono-substitution was observed in all the cases. The absence of dibenzoylated products can be attributed to the deactivating nature of the RCO group,

Table 3
Correlation of the catalytic activity with Lewis acidity

Calcination temperature (°C)	Perylene adsorbed (10^{-6} mol/g)	Conversion (%)
500	1.013	8.56
550	1.592	15.12
600	2.163	23.72
650	2.981	49.83
700	3.673	79.61

Reaction temperature: 110 °C; duration: 1 h; catalyst Fe(2)SZ: 0.1 g; toluene: benzoyl chloride molar ratio 5:1.

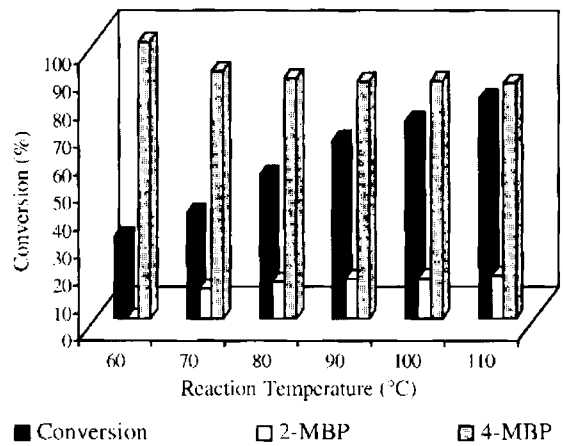

Fig. 6. Benzoylation of toluene with benzoyl chloride—influence of reaction temperature. Molar ratio (toluene:benzoyl chloride)—5:1; catalyst—Fe(2)SZ (0.1 g); duration—1 h.

after the introduction of which the reaction comes to a stop. Benzoylation of benzene results in the formation of benzophenone. In the case of toluene, *ortho*- and *para*-methylbenzophenones (2-MBP and 4-MBP) were obtained with around 84% selectivity to the *para* isomer. 3,4-Dimethylbenzophenone (3,4-DMBP) and 2,3-dimethylbenzophenone (2,3-DMBP) result from the aromatic substitution of *ortho*-xylene, the 3,4-isomer being formed with a selectivity of about 89%. The higher selectivity towards the *para* isomer in the case of xylene can be attributed to the steric hindrance of the two methyl groups.

The influence of reaction temperature on the percentage conversion and selectivity was followed for toluene and xylene; the results are illustrated in Figs. 6 and 7. In the case of toluene, 100% selectivity to the *para* isomer was obtained at 60 °C. Formation of *ortho* isomer was also observed above 70 °C. An increase in the reaction temperature resulted in an increase in the conversion at the expense of selectivity. At the refluxing temperature, *para* isomer was obtained with a selectivity of about 85%. In the case of xylene, 3,4-DMBP was the only product when reaction was carried out at 60 and 70 °C. As the reaction temperature was raised, the selectivity was lowered, and at refluxing temperature, around 89% of 3,4-DMBP was formed.

The influence of reaction time on the reactivity and selectivity for the benzoylation of xylene is illustrated

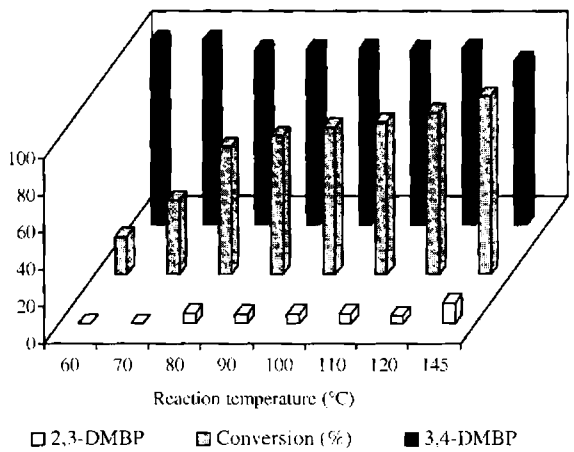

Fig. 7. Benzoylation of xylene with benzoyl chloride—influence of reaction temperature molar ratio (xylene:C_6H_5COCl)—5:1; catalyst—Fe(2)SZ (0.1 g); duration—1 h.

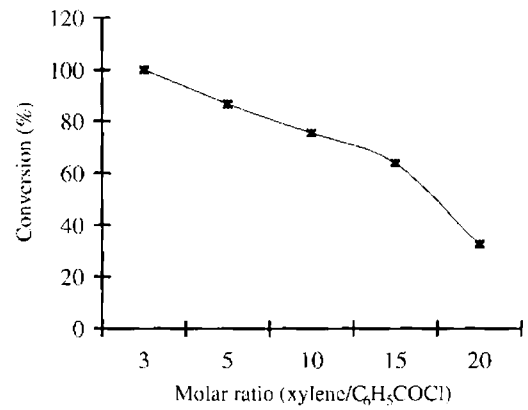

Fig. 9. Dependence of conversion percentage on molar ratio reaction temperature—110 °C; duration—1 h; Fe(2)SZ catalyst—0.1 g molar ratio (toluene:benzoyl chloride)—5:1.

in Fig. 8. The continuous increase in percentage conversion was registered with increase in reaction time, while the selectivity remained constant.

Molar ratio had a marked influence on the reaction rate. The reactivity was scanned for different molar ratios; the results are shown in Fig. 9. An increase in the toluene to benzoyl chloride ratio resulted in lowering of the reactivity. A drastic decrease in the percentage conversion was observed when the molar ratio was changed from 15:1 to 20:1. Traces of secondary reaction products could be detected at toluene: benzoyl chloride ratio of 3:1.

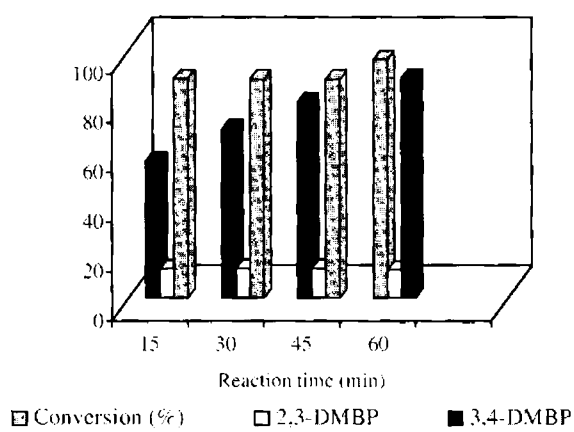

Fig. 8. Variation in conversion and selectivity with reaction time—benzoylation of xylene with benzoyl chloride. Reaction temperature—110 °C; 0.1 g Fe(2)SZ catalyst; duration—1 h; molar ratio (xylene:benzoyl chloride)—5:1.

The reusability of the catalyst systems was also subjected to investigation. The catalyst was removed by filtration from the reaction solution, washed thoroughly with acetone and then dried and activated. No pronounced change was observed in the XRD pattern, except for a slight lowering of intensity, symptomatic of the retention of the crystalline nature (Fig. 10). The systems were tested for catalytic activity and only a slight decrease was observed. This suggests the resistance to rapid deactivation acquired by the incorporation of iron. The absence of dark brown colour of the solution after the reaction points to the absence of Fe^{3+} in solution. To confirm this, the catalyst was filtered out and the reaction was continued for 15–30 min. No noticeable change in conversion could be detected, indicating the absence of metal leaching. The retention of the iron content was also confirmed by the EDX analysis of the sample after the reaction. At high iron loadings (Fe(10)SZ), a slight leaching out of the iron was observed by the EDX analysis (Fe content: 8.14%). However, the continued stirring after filtering of the catalyst failed to give any further reaction suggesting that the leached-out iron was inactive in catalysing the reaction. We conclude that any iron chloride formed by the probable reaction of the iron component of the catalyst with benzoyl chloride or HCl, which is evolved during

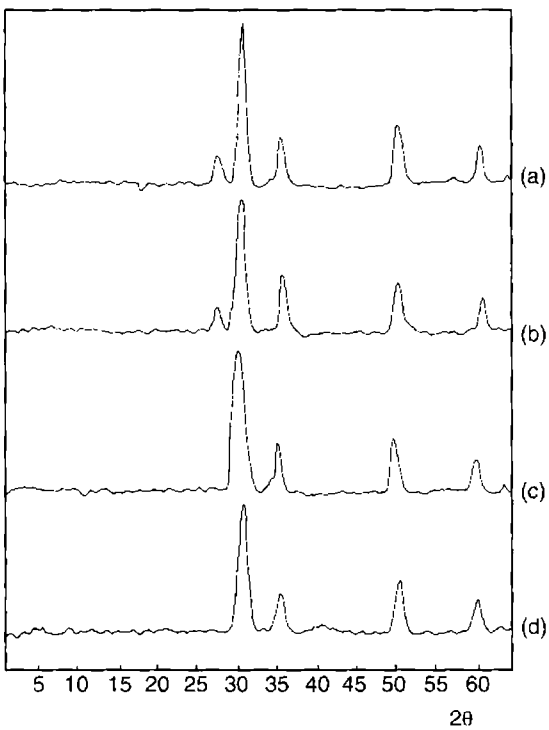

Fig. 10. XRD patterns of fresh and used representative samples: (a) Fe(2)SZ—fresh; (b) Fe(2)SZ—used; (c) Fe(10)SZ—fresh; (d) Fe(10)SZ—used.

the reaction, exists on the catalyst surface. Thus, the reaction can be assumed to be mainly heterogeneous in nature.

Acknowledgements

The financial support from CSIR to H. Suja and K. Sreeja Rani is gratefully acknowledged.

References

[1] G.A. Olah, Friedel–Crafts and Related Reactions, Vols. 1–4, Wiley/Interscience, New York, London, 1963–1964.
[2] G.A. Olah, Friedel–Crafts Chemistry, Wiley/Interscience, New York, London, 1973.
[3] U. Freese, F. Heinrich, F. Roessner, Catal. Today 49 (1999) 237.
[4] B. Jacob, S. Sugunan, A.P. Singh, J. Mol. Catal. A: Chem. 139 (1999) 43.
[5] A.X. Li, T.S. Li, T.H. Ding, Chem. Commun. (1997) 1389.
[6] G.A. Olah, R. Malhotra, K.S.C. Narang, J.A. Olah, Synthesis (1978) 672.
[7] K. Arata, M. Hino, Appl. Catal. 59 (1990) 197.
[8] M. Hino, K. Arata, J. Chem. Soc., Chem. Commun. (1985) 112.
[9] M. Miao, W. Hua, J. Chen, Z. Gao, Catal. Lett. 37 (1996) 187.
[10] M. Scheithauer, E. Bosch, U.A. Schubert, H. Knozinger, T.K. Cheung, F.C. Jentoft, B.C. Gates, B. Tesche, J. Catal. 177 (1998) 137.
[11] J.A. Moreno, G. Poncelet, Appl. Catal. A: Gen. 210 (2001) 151.
[12] M. Hino, Catal. Lett. 34 (1996) 125.
[13] X. Song, A. Sayari, Catal. Rev. Sci. Eng. 38 (3) (1996) 329.
[14] D. Farcasiu, J.Q. Li, S. Cameron, Appl. Catal. A 154 (1997) 173.
[15] G.D. Yadav, J.J. Nair, Micropor. Mesopor. Mater. 33 (1999) 1.
[16] C. Morterra, G. Cerrato, C. Emanuel, V. Bolis, J. Catal. 142 (1993) 349.
[17] A. Clearfield, G.P.D. Serrete, A.H. Khazi-Syed, Catal. Today 20 (1994) 295.
[18] L.M. Kustov, V.B. Kazansky, F. Figueras, D. Tichit, J. Catal. 150 (1994) 143.
[19] P.D.L. Mercera, J.G. van Ommen, E.B.M. Doesburg, A.J. Burggraaf, J.R.H. Ross, Appl. Catal. A 57 (1990) 127.
[20] F. Arena, R. Dario, A. Parmaliana, Appl. Catal. A: Gen. 170 (1998) 127.
[21] J. Kijenski, A. Baiker, Catal. Today 5 (1989) 1.
[22] B. D, J.A. N, R.C. Pink, Trans. Faraday Soc. 62 (1966) 730.
[23] R.T. Sanderson, Chemical Bonds and Bond Energy, Academic Press, New York, 1976, p. 75.
[24] H. Matsuhashi, H. Motoi, K. Arata, Catal. Lett. 26 (1994) 325.
[25] J.S. Lee, D.S. Park, J. Catal. 120 (1989) 46.
[26] A. Corma, C. Rodellas, V. Fornes, J. Catal. 88 (1984) 374.
[27] H.A. Benesi, J. Catal. 28 (1973) 176.
[28] H. Knozinger, H. Krietenbrink, P. Ratnasamy, J. Catal. 48 (1977) 436.
[29] J. Dewing, G.T. Monks, B. Youll, J. Catal. 44 (1976) 226.
[30] A. Satsuma, Y. Kamiya, Y. Westi, T. Hattori, Appl. Catal. A: Gen. 194/195 (2000) 253.
[31] C. Morterra, G. Cerrato, F. Pinna, M. Signoretto, J. Phys. Chem. 98 (1994) 12373.